1967-12

Experimental Analysis of a Plastic Model Multicell Cantilever Box Beam With 30° Sweep.

Sheler, James Anderson

Monterey, California. U.S. Naval Postgraduate School

http://hdl.handle.net/10945/12148

EXPERIMENTAL ANALYSIS OF A PLASTIC MODEL MULTICELL CANTILEVER BOX BEAM WITH 30° SWEEP

JAMES ANDERSON SHELER

EXPERIMENTAL ANALYSIS OF A PLASTIC MODEL

MULTICELL CANTILEVER BOX BEAM

WITH 30° SWEEP

by

James Anderson Sheler
Lieutenant, United States Navy
B.S., University of Washington, 1961

[redacted]

Submitted in partial fulfillment of the
requirements for the degree of

MASTER OF SCIENCE IN AERONAUTICAL ENGINEERING

from the

NAVAL POSTGRADUATE SCHOOL
December 1967

ABSTRACT

An experimental analysis of a plastic model four-cell swept back wing is presented. The model is cantilevered with a massive root rib oriented 60° with the spars. Three other ribs are located perpendicular to the spars. The results were compared with results previously obtained from tests performed on an aluminum alloy model of the same structure. Spanwise stresses and deflections compared very well. Considerable error was observed in chordwise stresses and shear stresses due to lack of joint duplication at the root rib and a difference in Poisson's Ratio between the two materials.

TABLE OF CONTENTS

CHAPTER		PAGE
I.	INTRODUCTION	11
II.	THE MODEL	13
	Selection	13
	Fabrication	14
	Instrumentation	19
III.	PREVIOUS TESTS AND METHODS OF COMPARISON	23
IV.	THEORETICAL CONSIDERATIONS	26
V.	TEST PROCEDURE	27
VI.	DISCUSSION OF RESULTS	32
VII.	CONCLUSIONS AND RECOMMENDATIONS	44
BIBLIOGRAPHY		47
APPENDIX I.	DETERMINATION OF MECHANICAL PROPERTIES OF PLEXIGLAS	49
APPENDIX II.	DESIGN EQUATIONS FOR STRUCTURAL SIMILARITY	55
APPENDIX III.	TORSIONAL SHEAR FLOW CALCULATIONS	58
APPENDIX IV.	DETERMINATION OF PRINCIPAL STRESSES AND PRINCIPAL AXES ORIENTATION	62

[illegible]

LIST OF TABLES

TABLE		PAGE
I.	Comparison of Stresses in Extreme Outer Fibre of Tension Cover Plate for One Pound Load. Loading Condition 1	33
II.	Comparison of Stresses in Extreme Outer Fibre of Tension Cover Plate for One Pound Load. Loading Condition 2	34
III.	Comparison of Stresses in Extreme Outer Fibre of Tension Cover Plate for One Pound Load. Torsion Loading	35
IV.	Comparison of Principal Stresses. Loading Condition 1	38
V.	Comparison of Principal Stresses. Loading Condition 2	39

[illegible]

[illegible] [illegible]

[illegible]

[illegible] [illegible]

[illegible] [illegible]

[illegible] [illegible]

[illegible] [illegible]

[illegible] [illegible]

LIST OF FIGURES

FIGURE		PAGE
1.	Model Planform	15
2.	Model Cross Section	16
3.	Rib and Spar Detail	17
4.	Cantilever End Detail	20
5.	Strain Gage Locations	21
6.	Loading Conditions	24
7.	Complete Test Setup	29
8.	Deflection Test Setup	30
9.	Comparison of Chordwise Stresses at Section A	37
10.	Deflections, Test 1, One Pound Load	41
11.	Deflections, Test 2, One Pound Load	42
I-1.	Tension vs Compression Test to Determine Modulus of Elasticity	50
I-2.	Creep Response Constant Stress	51
I-3.	Stress vs Strain Determination of Young's Modulus	53
I-4.	Determination of Poisson's Ratio	54
III-1.	Shear Flow at a Typical Cross Section	58
IV-1.	Rosette Orientation	62

[illegible]

TABLE OF SYMBOLS

A	area (in^2)
c	distance from the bending axis to extreme outer fibre (in)
E	modulus of elasticity (psi)
e	strain (in/in)
G	modulus of rigidity (psi)
γ	shear strain (in/in)
μ	Poisson's Ratio
μ_{Pb}	ratio of modulus of elasticity of plastic to modulus of elasticity of aluminum
I	rectangular moment of inertia (in^4)
J	section form factor-torsion (in^4)
l	length (in)
M	bending moment (in-lbs)
N_l	prototype lengths/model lengths
N_f	prototype forces/model forces
P	load (lbs)
q	shear flow (lbs per in)
σ	stress (psi)
τ	shear stress (psi)
T	torque (in-lbs)

CHAPTER I

INTRODUCTION

The problems associated with low aspect ratio, highly swept-back wings of today's modern high speed aircraft require extensive theoretical analyses and the use of costly electronic computers. Often, the theories employed and the associated assumptions made lead to large errors and uncertainties which would require experimental verification. This would usually require a full-scale prototype of the wing to be constructed for structural analysis purposes.

The cost and time involved in the construction of a full-scale model or even a scaled down model are often prohibitive. This is especially true in modern wing structures where milled cover skins and tapered spars and ribs are employed. The Saab Aircraft Company of Sweden considered the use of plastic models for their prototypes as early as 1953.[1] Other investigations into the use of plastic structural models began as early as 1943 in England.[2] Many errors were involved in these early analyses due to the relatively unfamiliar mechanical properties of the plastics and the methods of obtaining data. The results obtained were favorable with theory, but very few comparisons were made between the models and the actual structures being duplicated.

The objective of this thesis effort was to construct and analyze a plastic model of a four cell cantilever box

beam with 30° sweep and to correlate the results with previous tests of the same model constructed of 24ST aluminum alloy.[3,4]

This thesis was completed during the 1967-1968 academic year at the Naval Postgraduate School. Acknowledgement is gratefully made to Professor C. H. Kahr of the Aeronautics Department for his guidance as thesis advisor, and Mr. R. A. Besel, Mr. T. B. Dunton, and Mr. G. I. Gulbranson, structural laboratory technicians, for their assistance in the construction and instrumentation of the project.

CHAPTER II

THE MODEL

Selection:

The objective of this thesis effort was to construct and analyze a plastic model of a multi-spar, swept aircraft wing. The original selection was a scaled down model of the Chance Vought F8U-3 wing currently under investigation in the Aeronautical Structures Laboratory of the Naval Postgraduate School. The wing consisted of seven spars tapered in width and height, cambered cover plates tapered in both the spanwise and chordwise directions, and three ribs tapered in the chordwise direction. This model was rejected mainly due to the complexity of fabrication with no guaranteed results.

Being the initial project of this type undertaken at the Naval Postgraduate School, a simpler model had to be selected as the basic structure. The model selected was a four cell model wing with 30° sweep, consisting of two identical untapered cantilever beams joined together with a relatively stiff root rib. Each cantilever was of constant rectangular cross section with ribs oriented perpendicular to the spars. The top and bottom cover plates extended unbroken from tip to tip. It was constructed of 24ST aluminum alloy, and all components were joined with metal structural adhesives. Adhesives were used rather than metal fasteners to avoid stress concentrations, slip of the joints, and other irregularities in the load distributions.

A complete description and an experimental analysis of the basic model are contained in Reference 4.

The root rib of the basic model was a solid aluminum bar with cross section dimensions much greater than any of the other components. This was taken into consideration in the design of the plastic model with the prospect of constructing a half-span cantilever model. The relative size of the root rib should limit rotation at the built-in end so that deflections of the structure are affected very little.

Reference 5 describes an experiment performed on a plastic cantilever model with similar root rib characteristics. For a model with no sweep angle, a cubic proportionality was shown between displacement under a force and the distance of its point of application from the root rib. This is an agreement with theory, with the exception of a proportionality constant. The construction of a half-span cantilever model appears to be justified.

Fabrication:

Based on the above considerations, the decision was made to construct a half-span cantilever model with dimensions identical to those of the basic model, paying particular attention to the design of the built-in end.

Figures 1, 2, and 3 depict the planform, cross section, and the rib and spar detail respectively. All dimensions are the same as those of the basic model with the exception of the cover plate, spar and rib web thicknesses. The

FIG. 1

MODEL PLANFORM

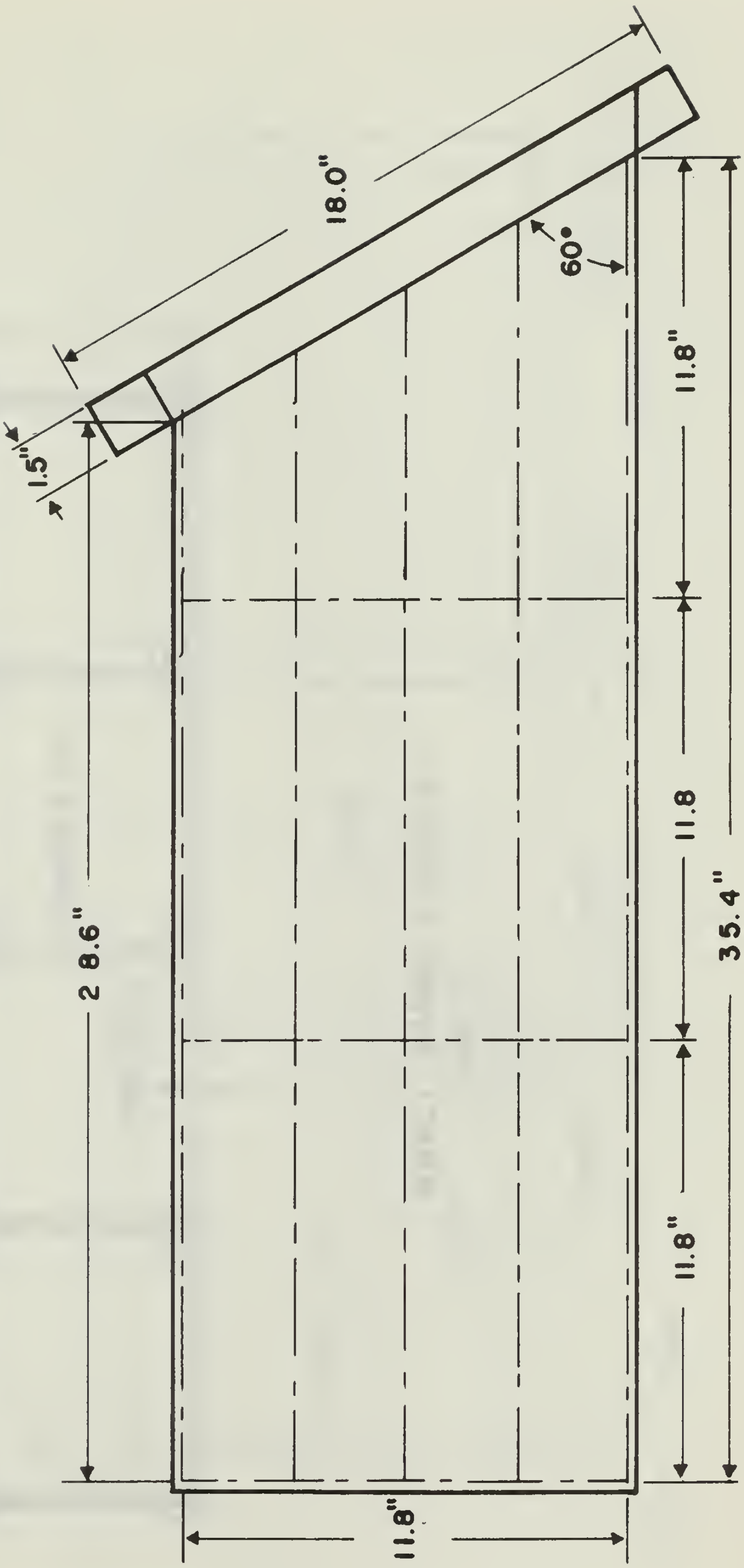

FIG. 2
MODEL CROSS SECTION

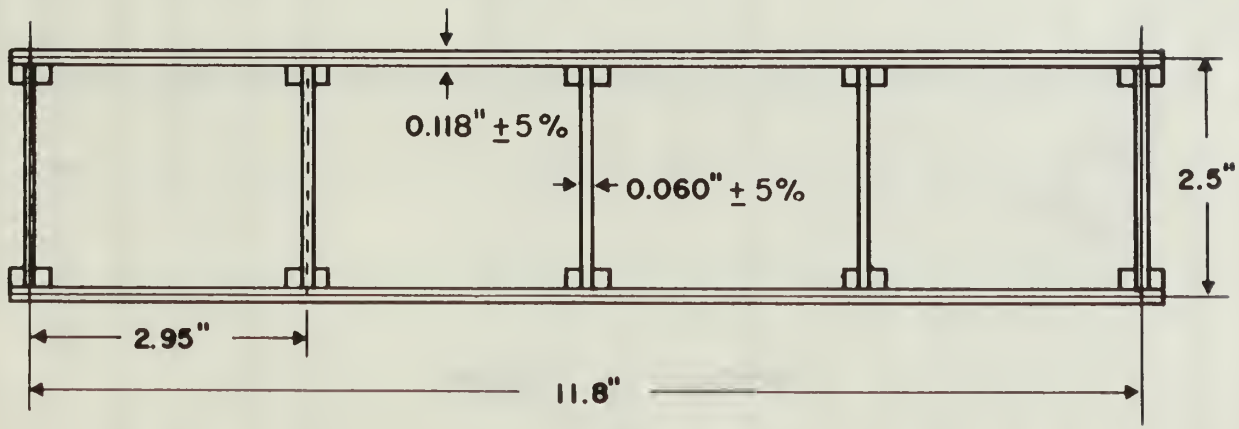

FIG. 3
RIB AND SPAR DETAIL

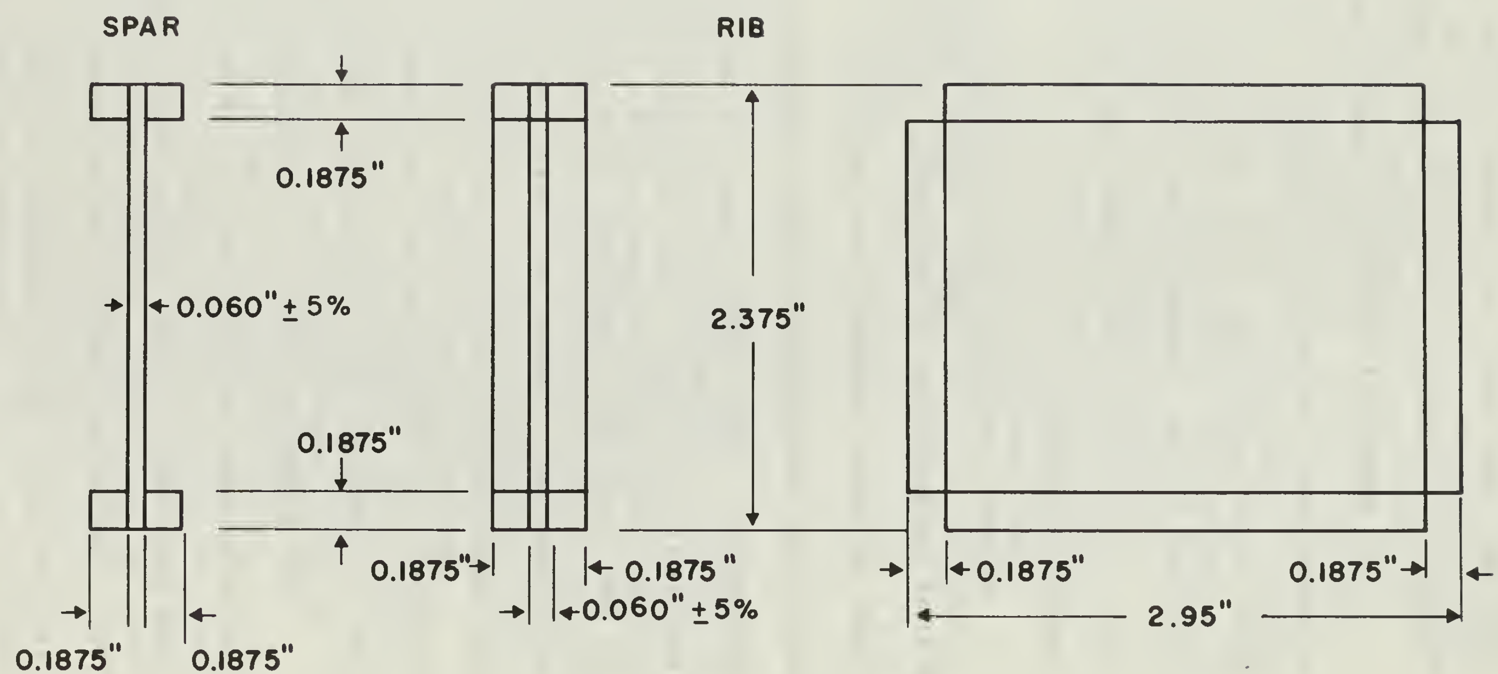

average thickness of the cover plates was 0.118 and 0.115 inch for the upper and lower plates respectively. The average thickness of the rib and spar webs was 0.062 inch.

The material used for constructing the model was methyl methacrylate, an acrylic plastic often called "Plexiglas G." Tests were performed on a small cantilever box beam constructed of the material to determine its mechanical properties. Appendix I describes the tests performed and the results obtained.

A more accurate and thorough investigation of the mechanical properties is desirable including glued specimens where solvent cements are employed. Previous experiments have been conducted on other types of plexiglas glued-joint specimens.[7] The effect was a lowering of the modulus of elasticity by 5 per cent for small glue joints and up to 100 per cent for laminated glue joints. Reference 8 describes the effects of using solvent cements for strain gage applications as well as for glue joints. Again the results vary depending on the size of the glued area, the type of cement, the materials, and the curing time allowed.

The adhesive used in constructing the model was methylene chloride, a quick-drying solvent cement, employing the "soak process." Glue joints were small in comparison to other dimensions except in the area of the root rib. Ventilation holes were provided in the ribs and some of the spars to lower the effects of solvent penetration into the areas surrounding the glue joints and to hasten the curing

time. The root rib has a large overlap area with the cover plates where the effect of the solvent could be pronounced.

The construction of the cantilever end is shown in Figure 4. The root rib is a solid bar of acrylic plastic 1.50 inches wide and 2.375 inches high. The rib is mounted on a one-half inch thick steel backing plate by means of six one-half inch diameter bolts. Four screw plates, 2 x 2 x 1/8 inches are mounted on the inside of the rib to aid in distributing the load. The entire structure was then mounted on a massive upright steel girder to give further stiffness to the built-in end.

Instrumentation:

Resistance type strain gages were located as shown in Figure 5. Type FABR-12-12 strain gage rosettes were used at section G, employing only the perpendicular elements in the spar shear webs. All other gages are type FAER-25R-12S13L strain gage rosettes. Only the upper cover plate was instrumented due to the symmetry of the model. All gages were mounted with cyanoacrylate cement (Eastman 910), a quick-drying cement that requires no curing process.

Foil type, 120 ohm strain gages were selected for the model to minimize gage current effects and to aid in heat dissipation. Large errors may occur due to the lack of heat dissipation when gages are mounted on poor conductors such as plastics. Gage current also effects the time required for temperature equilibrium to be reached. Both

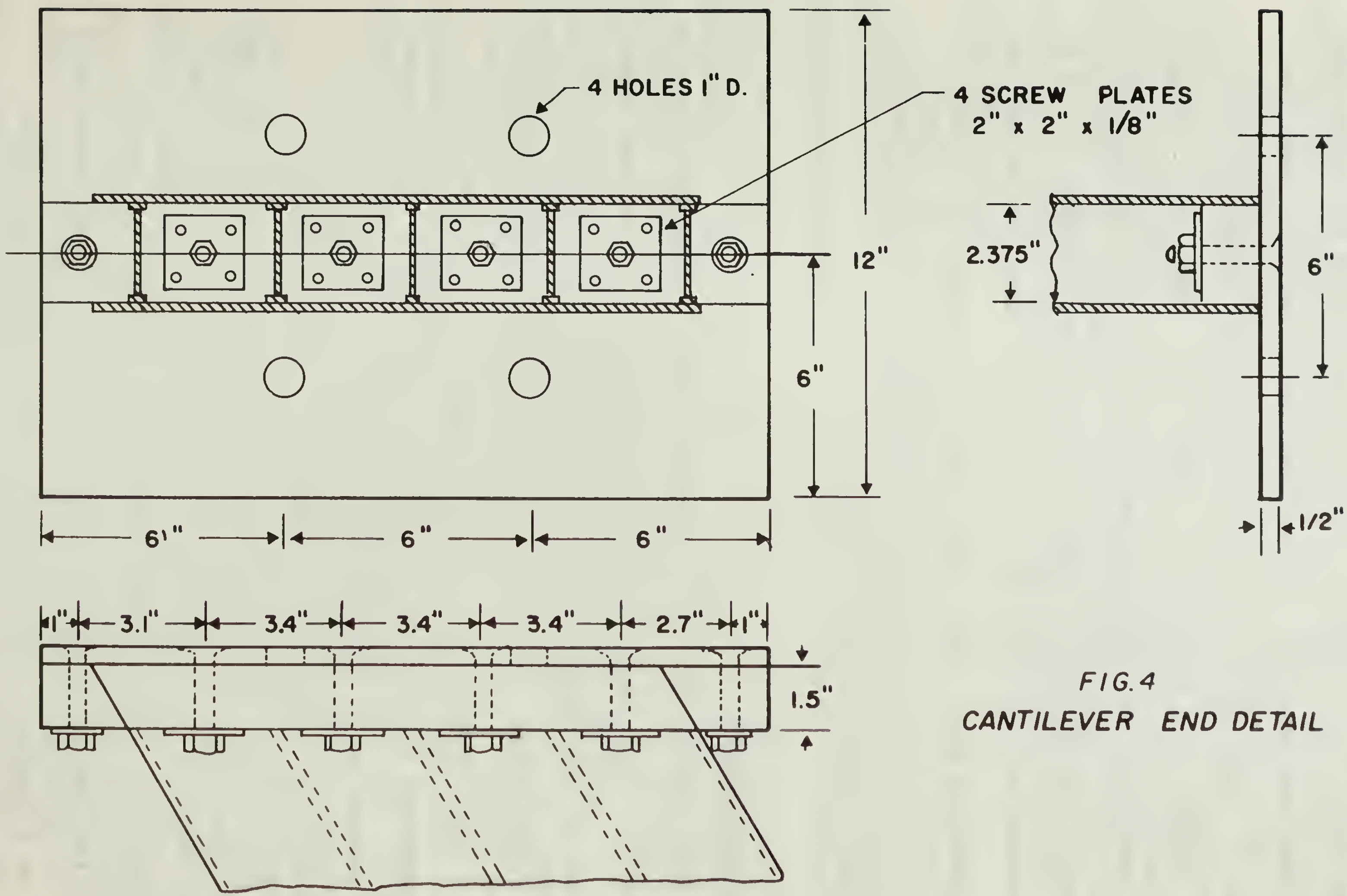

FIG. 4
CANTILEVER END DETAIL

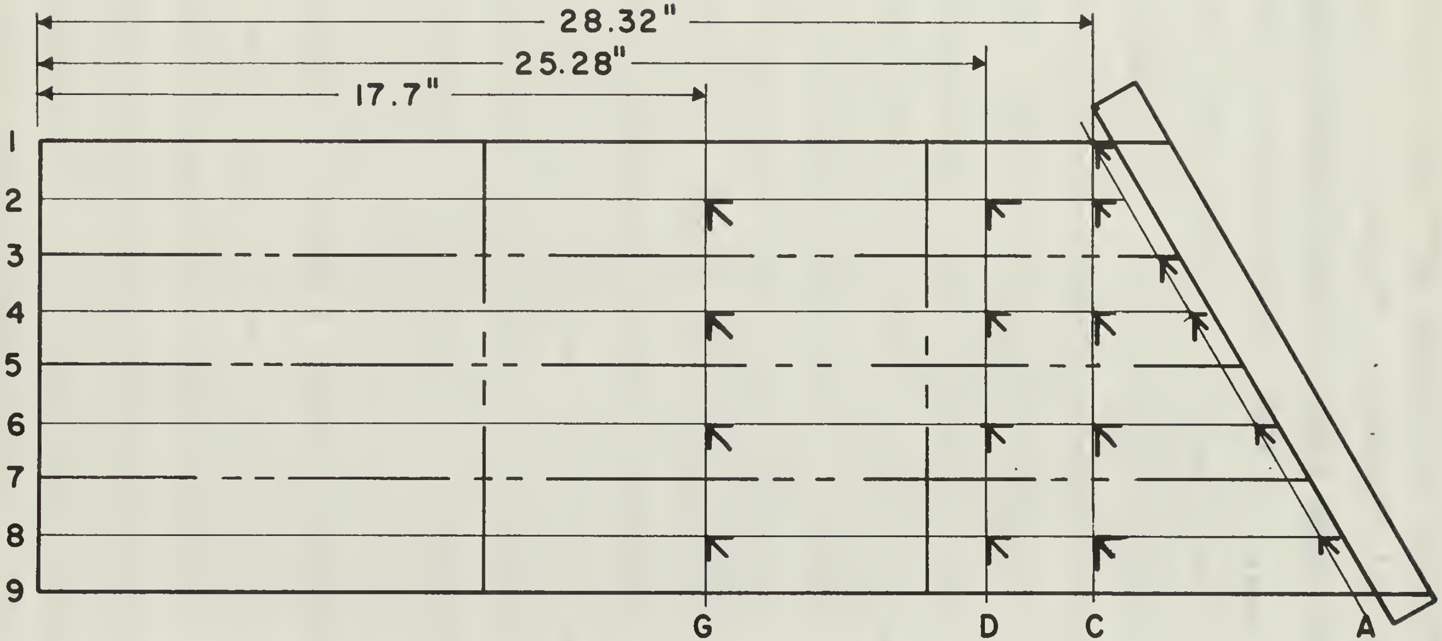

2 Element Rosettes Located
On All Spar Webs At Section G

FIG. 5
STRAIN GAGE LOCATIONS

of these effects are minimized by employing foil type gages.[9] Reference 10 describes gage current effects on plastic models and recommends the use of 120 ohm gages only. The higher resistance gages require higher currents and thus generate more heat.

CHAPTER III

PREVIOUS TESTS AND METHODS OF COMPARISON

The tests performed on the basic model are described in Reference 4 and are summarized below.

The stress distribution was determined for two different loading conditions. In the first condition, the loading points were at the intersection of the tip rib and the front and rear spars; and, in the second condition, at the intersection of the rear spar and the tip rib only. See Figure 6.

The loads applied were 750 kgs for loading condition 1 and 680 kgs for loading condition 2. The mean values obtained from three test runs were employed to determine the stress distribution. These values were reduced to the unit load case in the English system for comparison with values obtained from tests performed on the plastic model. The torsion loading case was obtained by subtracting the results of loading condition 1 from those of loading condition 2.

Exact structural characteristics could be obtained from the plastic model if it was a complete geometric duplication of the basic model, and if the differences in the mechanical properties are taken into consideration. Reference 6 lists the design equations to be used for structural similarity. These equations are summarized in Appendix II. Assuming complete geometric duplication, it is observed that if bending deflections of the basic model are to be reproduced, the forces on the plastic model have to be reduced by

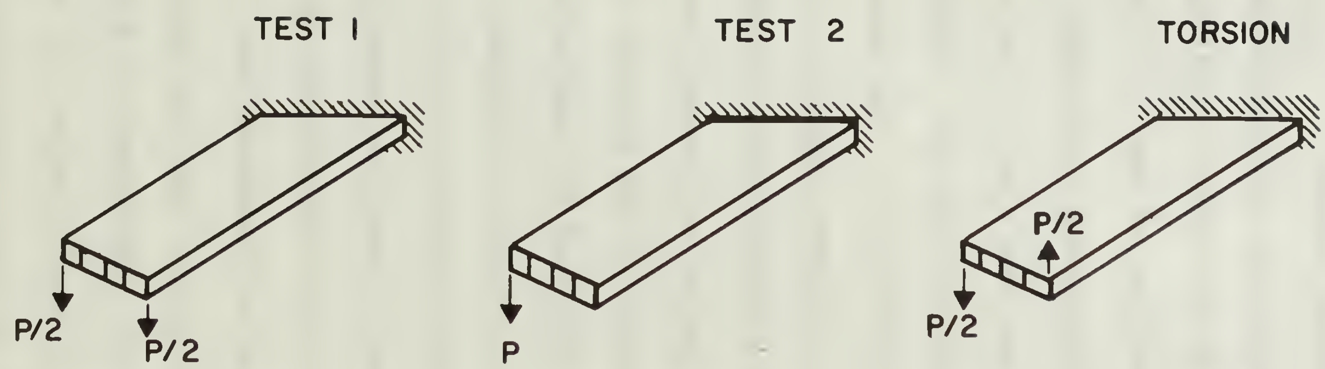

FIG. 6

LOADING CONDITIONS

a ratio of the modulus of elasticity of the plastic to the modulus of elasticity of the aluminum (μ_{pb}). This is shown in Equations (II-1a) and (II-2a) of Appendix II. Equation (II-3a) implies that, if torsional deflections are to be reproduced, the forces have to be reduced by a ratio of the torsional rigidities. This includes both Poisson's Ratio and the modulus of elasticity of the materials.

For the cases under consideration, bending stresses, shear stresses, and bending deflections are to be compared. Equations (II-4a), (II-5a), (II-6a), and (II-7a) imply that the ratio of the stresses in the plastic model to those of the basic model is equal to the ratio of the respective loadings, assuming complete geometric duplication. Bending deflections will vary inversely with μ_{pb}.

All of the important dimensions of the basic model have been reproduced in the plastic model with the exception noted previously; therefore, geometric duplication can be assumed. The results obtained from the tests on the plastic model can be compared to the results of the basic model as stated above.

CHAPTER IV

THEORETICAL CONSIDERATIONS

Several theoretical analyses have already been performed on the basic model under the same loading conditions. It was analyzed first in Reference 3, employing the least-work method. Reference 11 analyzes the trailing edge of the same model in the vicinity of the root rib employing the direct-stiffness method. Reference 12 contains a complete stress-deflection analysis of the model employing the matrix-force method. A theoretical analysis of the plastic model would be useful due to the difference in Poisson's Ratio; however, it was considered beyond the scope of this report.

A torsional analysis at a cross section of the model has been performed and is contained in Appendix III. This method was also applied to check the accuracy of experimental results. The shear stresses at stations C, D, and G were converted to shear flows and substituted into Equation (III-4) of Appendix III to obtain the internal torsional moment. The results were compared to the applied external torsional moment to determine the experimental error.

CHAPTER V

TEST PROCEDURE

The problems of strain variation due to creep of the material and gage current effects have been mentioned previously. In order to keep the creep variations at a minimum it was necessary that all of the strains be measured at the same time. In this case the time chosen was ten minutes after load application, to correspond to the modulus of elasticity determined in Appendix I. To keep current effects at a minimum, it was necessary to have the current as low as possible for heat dissipation considerations and also to have current flowing through all of the gages during the test for temperature equilibrium considerations.

The test equipment for the analysis was selected to meet the above requirements. A variable power supply was employed to control the voltage and thus the current in the gages. The voltage was set at two volts. All gages, including the temperature compensating gages, were kept under power during the entire test. It should be noted that a decrease in current flow through a strain gage lowers the sensitivity of the gage. This was compensated for by amplifying the signal received from the gage by means of a direct-current amplifier.

A voltage-to-frequency converter used in conjunction with an electronic frequency counter was employed to convert the amplified strain signal to a digital strain read-out.

A ninety-nine channel scanner circuit with a balancing potentiometer for each channel was used to switch from one gage to another. A digital recorder was also provided which stepped automatically between gages. The time between steps could be controlled so that all gages were read within two minutes. This minimizes variations in strain readings due to material creep. Figure 7 shows the complete test setup with the model loaded as in load condition 1.

Deflection measurements were taken at the intersection of the ribs and outboard spars by means of mechanical dial indicators. The deflection test setup is shown in Figure 8. The dial indicators add small forces to the model at their points of application; therefore, it was necessary to use relatively large loads for the deflection tests.

Three test runs were made for each loading condition. The load for each case was 36.08 pounds. This kept the stress level below the 500 psi limit described in Appendix I. The mean values of the three tests were used to determine the stresses and deflections.

It was necessary to make gage factor corrections and gage cross-sensitivity corrections for all of the measured strains before reducing the data to the desired stresses. The method employed for data reduction is contained in Appendix IV. A previously compiled computer program was utilized for this purpose. The results were then reduced to the unit load case for each loading condition. The

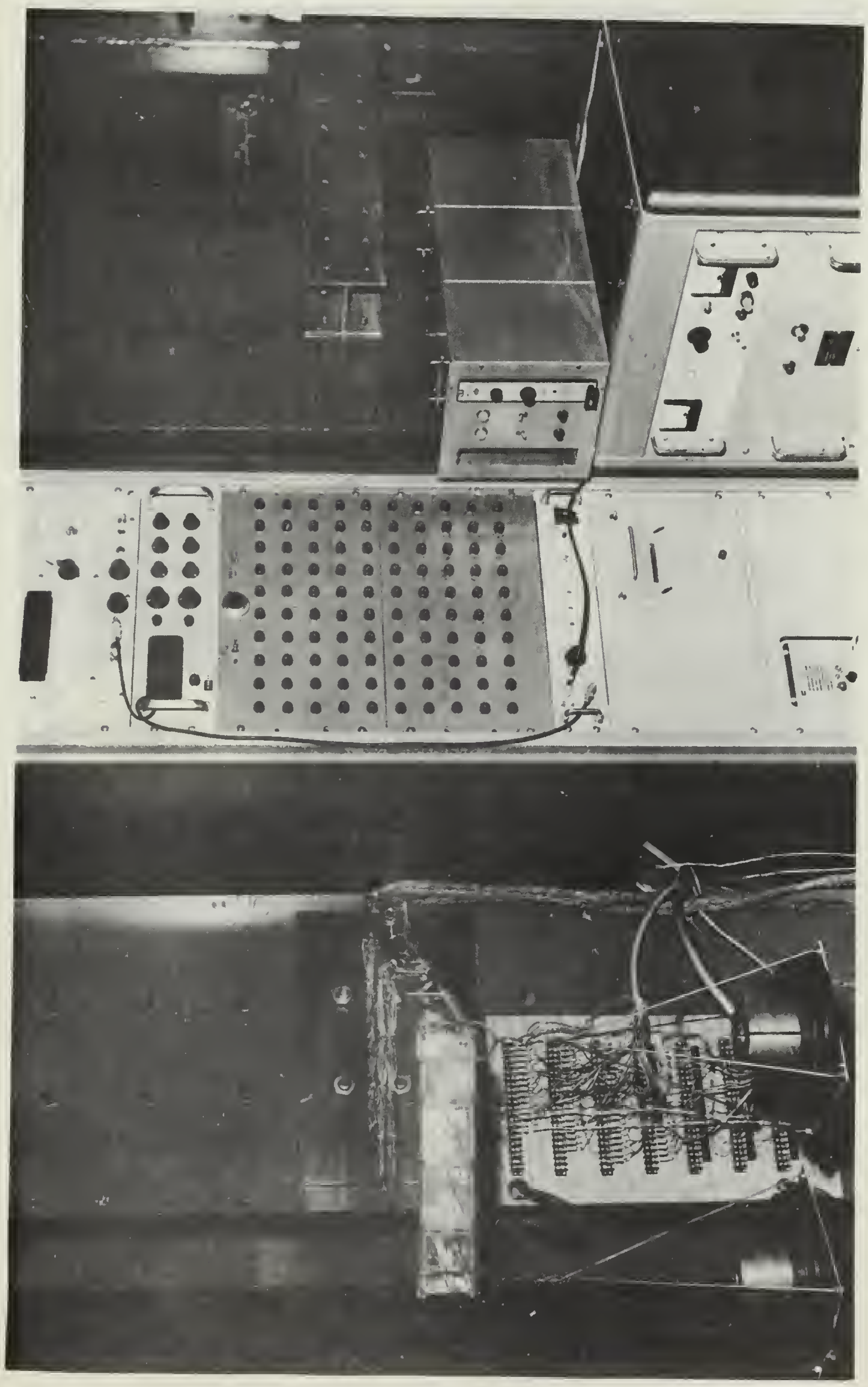

FIG. 7 [illegible]

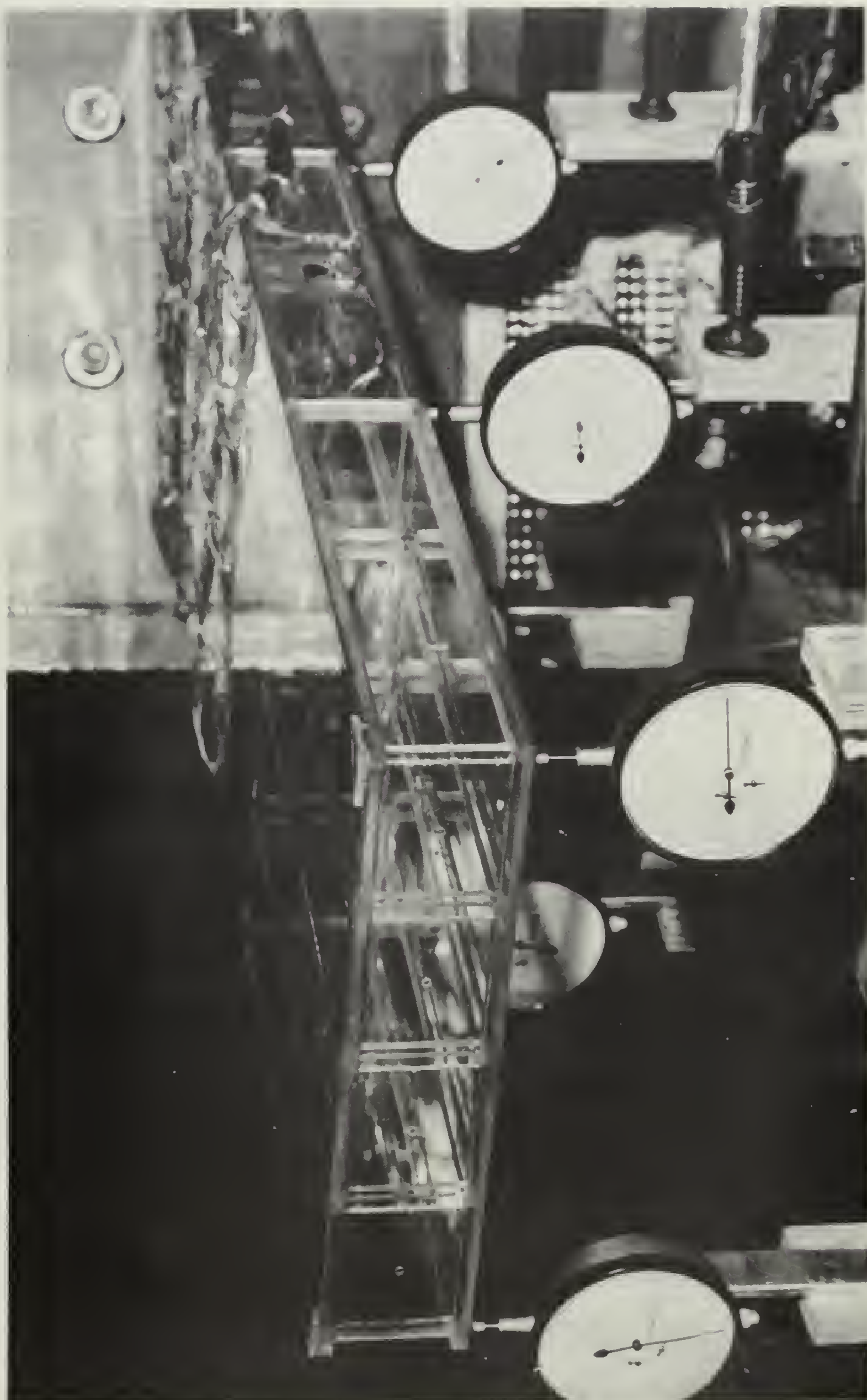

FIG. [illegible] DEFLECTION TEST [illegible]

torsion loading condition was obtained by subtracting the results of loading condition 1 from those of loading condition 2.

The deflection measurements were also reduced to the unit load case for comparison with the results of the basic model. The deflections of the basic model had to be multiplied by μ_{pb} for compatible results.

CHAPTER VI

DISCUSSION OF RESULTS

Tables I and II compare the experimental stresses of the two models for a unit load under loading conditions 1 and 2 respectively. Table III compares the torsional loading case.

A comparison of the spanwise bending stresses shows that the plastic model has somewhat higher values than the basic model with one exception. The exception occurs where the values were obtained from a strain gage mounted on the underside of the tension cover sheet. Gages were mounted on both sides of the cover sheet at this station in order to determine the bending stress distribution in the sheet; however, the gage on the upper surface was damaged. The lower values obtained on the underside of the cover sheet were expected since the bending stress is proportional to the distance from the neutral axis of the cross section.

The bending stresses near the rib root section had errors ranging from +7 per cent at station A1 to +26 per cent at station A6 for loading condition 1, and 2.5 per cent at station A8 to 21 per cent at station A6 for loading condition 2. These gages are all located at 0.28 inch from the rib root section. In this vicinity it is possible that the solvent from the large glue joint of the center section has affected the modulus of elasticity of the material. Away from the root rib section, the spanwise bending

TABLE I

COMPARISON OF STRESSES IN EXTREME OUTER FIBRE OF TENSION COVER PLATE FOR ONE POUND LOAD. LOADING CONDITION I.

REF. POINT	σ_y (psi)	σ_x (psi)	τ_{xy} (psi)
	BASIC MODEL		
A1	12.447	0.450	-0.651
A3	7.210	-0.561	-1.219
A4	6.823	0.471	-1.135
A6	5.127	0.090	-0.774
A8	4.127	-0.271	-0.168
C4	6.520	0.135	-1.019
C6	5.301	-0.174	-0.845
C8	4.630	-0.310	-0.438
D2	6.965	0.316	-0.890
D4	5.959	-0.290	-1.090
D6	5.114	0.019	-0.993
D8	4.824	-0.509	-0.767
G2	---	---	-0.148
G4	---	---	-0.058
G6	---	---	-0.110
G8	---	---	-0.135
	PLASTIC MODEL		
A1	13.339	3.832	-2.796
A3	8.250	2.113	-0.662
A4	7.558	1.461	-0.156
A6	6.500	0.626	-0.146
A8	4.905	0.211	-0.204
C4	6.256	1.181	-0.833
C6	5.868	0.832	-0.356
C8	4.902	0.129	-0.078
D2	7.763	0.194	-0.745
D4	6.142	0.492	-0.925
D6	5.556	0.471	-0.857
D8	5.115	0.196	-0.609
G2	4.209	-0.242	-0.161
G4	3.895	-0.361	-0.073
G6	3.699	-0.382	0.044
G8	3.646	-0.524	-0.351

TABLE II

COMPARISON OF STRESSES IN EXTREME OUTER FIBRE OF TENSION COVER PLATE FOR ONE POUND LOAD. LOADING CONDITION 2.

REF. POINT	σ_y (psi)	σ_x (psi)	τ_{xy} (psi)
	BASIC MODEL		
A1	13.220	-0.574	0.226
A3	7.397	-1.548	-0.671
A4	6.733	0.142	-0.516
A6	4.676	-0.097	-0.071
A8	3.502	-0.213	0.400
C4	6.372	0.200	-0.180
C6	4.837	-0.258	-0.161
C8	4.211	-0.026	0.271
D2	7.268	0.303	-0.123
D4	5.901	-0.123	-0.187
D6	5.082	0	-0.135
D8	4.708	-0.123	0.052
G2	---	---	0.922
G4	---	---	0.890
G6	---	---	0.819
G8	---	---	0.490
	PLASTIC MODEL		
A1	13.894	2.497	-1.821
A3	8.398	1.229	-0.156
A4	7.311	0.668	0.370
A6	5.670	0.030	0.219
A8	3.591	-0.382	0.554
C4	6.117	0.886	-0.112
C6	5.623	0.576	0.351
C8	4.633	0.094	0.409
D2	7.837	0.142	-0.097
D4	6.110	0.372	-0.102
D6	5.362	0.384	-0.054
D8	4.848	0.095	0.049
G2	4.326	-0.467	0.555
G4	4.018	-0.463	0.779
G6	3.576	-0.281	0.895
G8	3.624	-0.545	0.311

TABLE III

COMPARISON OF STRESSES IN EXTREME OUTER FIBRE OF TENSION COVER PLATE FOR ONE POUND LOAD. TORSION LOADING.

REF. POINT	σ_y (psi)	σ_x (psi)	τ_{xy} (psi)
	BASIC MODEL		
A1	0.773	-1.024	0.887
A3	0.187	-0.987	0.548
A4	-0.095	-0.329	0.619
A6	-0.451	-0.187	0.703
A8	-0.625	0.058	0.568
C4	-0.148	0.065	0.839
C6	-0.464	-0.084	0.684
C8	-0.419	0.284	0.709
D2	0.303	-0.013	0.767
D4	-0.058	0.167	0.903
D6	-0.032	-0.019	0.858
D8	-0.116	0.386	0.819
G2	---	---	1.070
G4	---	---	0.948
G6	---	---	0.929
G8	---	---	0.625
	PLASTIC MODEL		
A1	0.510	-1.335	0.975
A3	0.148	-0.884	0.506
A4	-0.247	-0.793	0.526
A6	-0.830	-0.596	0.635
A8	-1.314	-0.593	0.758
C4	-0.139	-0.295	0.721
C6	-0.245	-0.256	0.707
C8	-0.269	-0.035	0.487
D2	0.074	-0.052	0.648
D4	-0.032	-0.120	0.823
D6	-0.194	-0.087	0.803
D8	-0.267	-0.101	0.658
G2	0.117	-0.225	0.716
G4	0.123	-0.102	0.825
G6	-0.093	0.101	0.851
G8	-0.022	-0.021	0.662

stresses are all somewhat higher in the plastic model with the average error being +7.6 per cent. This may be attributed to a possible discrepancy in the determination of the modulus of elasticity of the material and experimental error.

A large discrepancy occurs in the comparison of chordwise axial stresses and shear stresses, especially near the root rib. The differences are due to a combination of shear lag, Poisson's strains, and rigidities of the built-in ends. The chordwise stresses near the root rib in the plastic model were considerably higher than those of the basic model. An inspection of Figure 9 reveals chordwise stress discontinuities in the basic model, not present in the plastic model. This would indicate a lack of joint duplication between the two models. The effects of these discontinuities are fed back into the structure and are still evident at section D. The shear distribution is affected in much the same manner; hence, comparison is impossible.

Away from the root rib, the difference in Poisson's strain has a noticeable effect on the chordwise stresses. It can be shown that the magnitude of these stresses is directly proportional to Poisson's Ratio and the spanwise strain. Poisson's Ratio of the plastic is 0.384 compared to 0.30 for the aluminum. Chordwise stress would, therefore, be higher in the plastic model.

Tables IV and V compare the principal stresses and the principal axes for the two models. The maximum principal

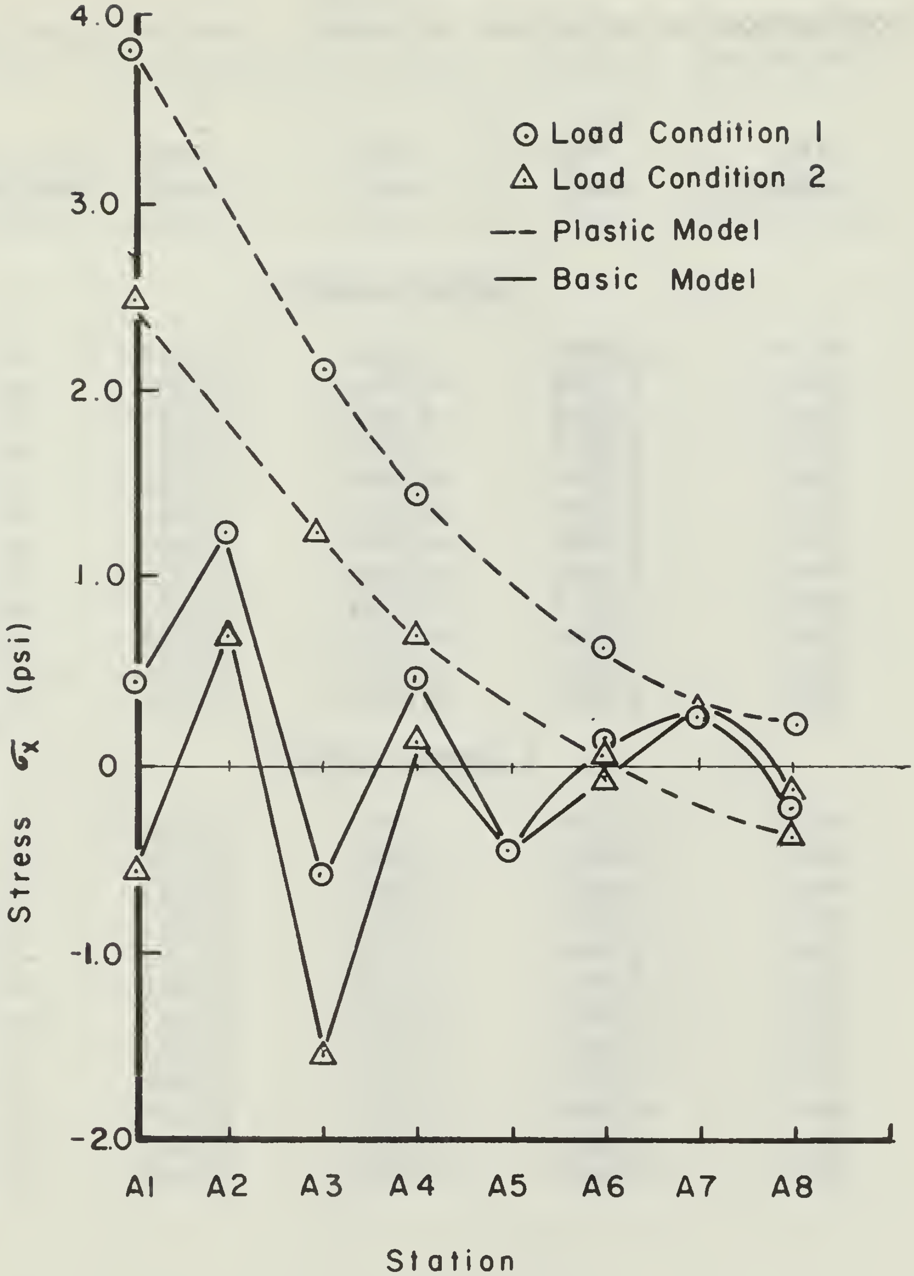

FIG. 9

COMPARISON OF CHORDWISE STRESSES AT SECTION A

TABLE IV

COMPARISON OF PRINCIPAL STRESSES. LOADING CONDITION 1

REF. POINT	σ_{max} (psi)	σ_{min} (psi)	τ_{max} (psi)	PRINCIPAL AXES DEGS.
		BASIC MODEL		
A1	12.490	0.406	6.030	+1.12
A3	7.420	-0.749	4.080	+8.67
A4	7.030	0.271	3.375	+9.87
A6	5.250	-0.026	2.539	+8.55
A8	4.150	-0.277	2.220	+2.20
C4	6.690	-0.026	3.360	+8.72
C6	5.440	-0.287	2.860	+8.60
C8	4.675	-0.348	2.515	+5.00
D2	7.090	-0.594	3.450	+8.87
D4	6.150	-0.477	3.320	+9.26
D6	5.300	-0.016	2.725	+10.67
D8	4.920	-0.593	2.760	+7.14
		PLASTIC MODEL		
A1	14.100	3.071	5.515	+15.23
A3	8.321	2.043	3.139	+6.09
A4	7.563	1.457	3.053	+1.46
A6	6.521	0.622	2.951	+2.83
A8	4.910	0.201	2.322	-6.83
C4	6.389	1.048	2.671	+9.09
C6	5.839	0.807	2.543	+4.02
C8	4.903	0.127	2.388	+0.94
D2	7.835	0.122	3.857	+5.57
D4	6.290	0.345	2.937	+9.07
D6	5.697	0.331	2.683	+9.32
D8	5.190	0.122	2.534	+6.95

TABLE V

COMPARISON OF PRINCIPAL STRESSES. LOADING CONDITION 2

REF. POINT	σ_{max} (psi)	σ_{min} (psi)	τ_{max} (psi)	PRINCIPAL AXES DEGS.
		BASIC MODEL		
A1	13.250	0.580	6.800	+0.50
A3	7.410	-1.445	4.520	+4.25
A4	6.780	0.103	3.340	+4.39
A6	4.670	-0.097	2.390	+1.35
A8	3.550	-0.258	1.900	-6.38
C4	6.380	0.200	3.095	-1.78
C6	4.840	-0.254	2.560	-1.71
C8	4.225	-0.045	2.135	-3.84
D2	7.280	0.297	3.490	+0.88
D4	5.900	-0.129	3.015	+2.08
D6	5.090	-0.013	2.555	+1.50
D8	4.710	-0.129	2.415	-0.87
		PLASTIC MODEL		
A1	14.178	2.213	5.983	+8.86
A3	8.401	1.225	3.588	+1.25
A4	7.331	0.647	3.342	-3.18
A6	5.672	0.023	2.787	-4.37
A8	3.764	-0.349	2.033	-1.97
C4	6.119	0.884	2.618	+1.23
C6	5.647	0.553	2.547	-3.96
C8	4.669	0.057	2.306	-5.11
D2	7.838	0.141	3.849	+0.73
D4	6.112	0.371	2.871	+1.02
D6	5.362	0.383	2.489	+0.62
D8	4.849	0.094	2.377	-0.59

stresses in the plastic model are greater in all cases with the exception of station C4 (The reason for the exception has been previously noted.). The error parallels the error in the spanwise stresses. The differences in the values of the minimum principal stresses and the orientation of the principal axes near the root rib tend to verify the discontinuities at section A. The decrease in maximum shear stress and the increase in minimum stress away from the root rib can be attributed to the difference in Poisson's Ratio of the two materials.

Figures 10 and 11 compare the deflections for the two loading cases. For loading condition 1, the deflections at the rear spar were exactly equal to those of the basic model. The deflections at the front spar were, on the average, 10 per cent lower. For loading condition 2, the deflections at the tip rib were less than 1 per cent different than those of the basic model. At the center rib the deflections were 23 per cent and 43 per cent greater in the plastic model for the front and rear spars respectively. The differences here can be attributed to the differences in torsional rigidities of the two materials. There will also be some effect from the discontinuities mentioned above.

To check the accuracy of the above experimental results, the shear flows at sections C, D, and G were determined from the torsional loading case and substituted into Equation (III-4) of Appendix III. This determined the

FIG. 10

DEFLECTIONS TEST I

ONE POUND LOAD

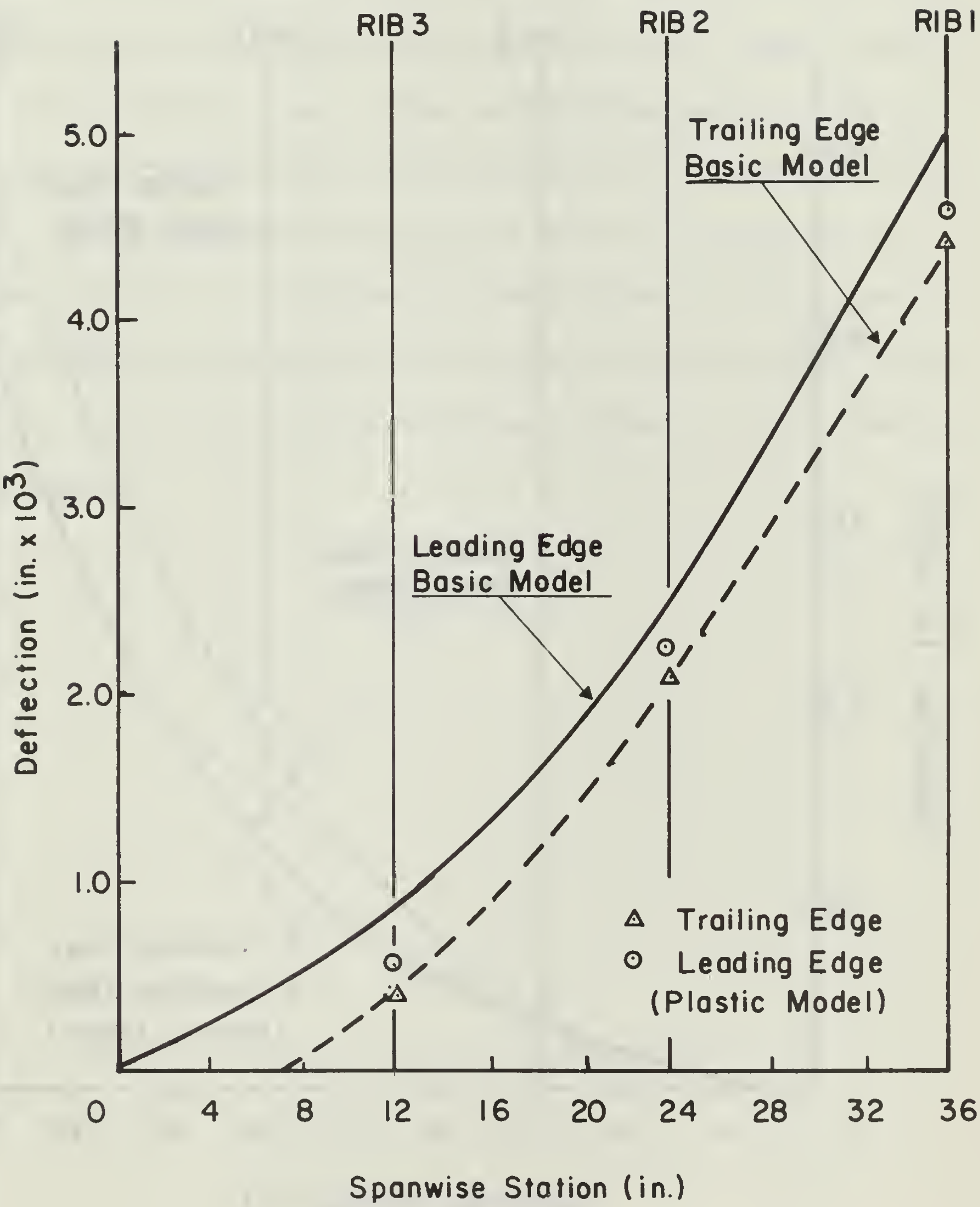

FIG. 11
DEFLECTIONS TEST 2
ONE POUND LOAD

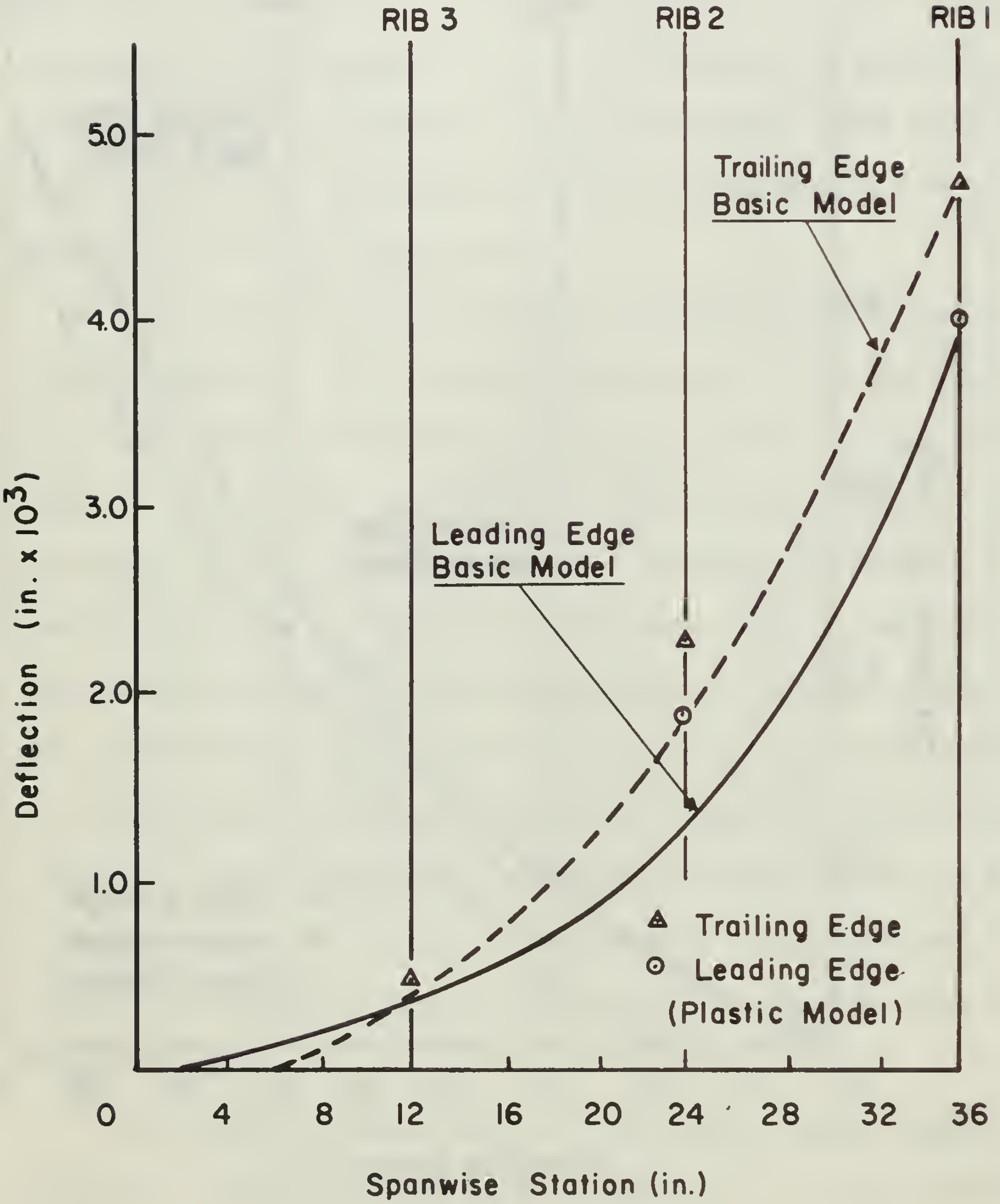

internal torsional moments at these sections. These moments were compared to the externally applied torsional moment. The error at section G, which is a considerable distance from the rib root section, was -2.4 per cent. At section D the error was -6.7 per cent, and at section C, which is extremely close to the root rib at the trailing edge, the error was only -14 per cent. The accuracy appears to be very good at section G where the assumptions of Appendix III are valid. These assumptions are not valid at section C because the section is not free to warp under torsion loading. The assumptions applied at section D are marginal and are probably invalid, although the calculated error is still relatively small.

CHAPTER VII

CONCLUSIONS AND RECOMMENDATIONS

The objective of this thesis effort was to construct and analyze a plastic model of a four-cell cantilever box beam with 30° sweep, and to correlate the results with previous tests of the same model constructed of aluminum alloy. The reason for the analysis was to investigate the feasibility of employing plastic structural models for stress and deflection tests in order to predict the structural characteristics of an actual structure. In this case the structure under consideration was a swept-back wing with emphasis being placed on the analysis in the region near the intersection of the root rib and the rear spar.

Based on results obtained, it is concluded that the plastic model could be used to accomplish the desired results if extreme care is taken in the construction of the model. The most important consideration is the duplication of all joints. This is necessary if shear and transverse stresses are to be compared.

Based on the results of the deflection tests, there appeared to be no slippage of the glue joints. Some evidence exists that the solvent glue may have affected the modulus of elasticity in the vicinity of the root rib. Large glue joints of this type should be avoided unless a non-solvent type adhesive is employed.

The deflections obtained agree very well with the deflections of the basic model in most cases. This would tend to indicate that a half-span cantilever model could be used in some cases. Usually, however, the root rib section cannot be duplicated by a cantilever model, and a full-span model should be used.

The strain readings varied up to $\pm$ 5 per cent from the mean values. The largest variations occurred at strain levels below 100 micro-inches. For accurate results, all tests should be run at the same temperature and a low humidity. Strain gage current should be kept as low as possible and yet maintain the sensitivity of the gage.

Poisson's Ratio of the plastic has a noticeable effect on test results. The results are conservative for axial and bending stresses but are non-conservative for maximum shear stresses. The effect would have to be taken into consideration if accurate results are desired.

Other errors could be introduced into the structure by inaccurate determination of the mechanical properties of the plastic, variations in thickness of the plastic, pre-stressing of joints, and methods of strain gage application. These are some of the more important error producing considerations.

The following recommendations are made for future endeavors in this area.

1. Ensure duplication of all joints.

2. Avoid the use of solvent-type adhesives for large glue joints; and, allow adequate ventilation and curing time for all solvent-type glue joints.
3. Use full-span models whenever practicable.
4. Make all strain gage tests under controlled atmospheric conditions.
5. Use 120 ohm foil type strain gages and maintain the gage current as low as possible, preferably below 10 ma.
6. Consider Poisson's Ratio effect for the different materials.
7. Use a higher grade plastic with better thickness tolerances.

BIBLIOGRAPHY

1. Noton, B. R. Experimental Investigation of the Stress Distribution in a Plastic Model of a 35° Swept Back Wing With Multi-web Construction. The Aeronautical Research Institute of Sweden, Report No. 47, Stockholm, 1953.

2. Redshaw, S. C., Palmer, P. J. "The Construction and Testing of a Xylonite Model of a Delta Aircraft," The Aeronautical Quarterly, Vol. III, September, 1951, pp. 83-127.

3. Eggwertz, Sigge. Calculation of Stresses in a Swept Back Cantilever Box Beam With Ribs Perpendicular to the Spars and Comparison to Test Results. The Aeronautical Research Institute of Sweden, Report No. 54, Stockholm, 1954.

4. Noton, B. R. Stress and Deflection Measurements on a Multicell Cantilever Box Beam With 30° Sweep. The Aeronautical Research Institute of Sweden, Report No. 53, Stockholm, 1954.

5. Hall, A H. "An Experimental Study of the Static Stiffness and Deformation of Swept Wings With Uniform Chord," Third Anglo-American Aeronautical Conference Brighton 1951, London, The Royal Aeronautical Society, 1952, pp. 525-544.

6. Raphiael, Coleman. "Considerations in the Design of Structural Models," Aeronautical Engineering Review, February, 1955, pp. 52-55.

7. Noton, B. R. "Structural Aspects of Swept-Back Wings," Aircraft Engineering, Vol. XXV, No. 297, November, 1953, pp. 330-343.

8. Eney, W. J. "Discussion of Paper Entitled Bonded Wire Strain Gage Techniques for Polymethyl Methacrylate Plastics," Proceedings of the Society for Experimental Stress Analysis, Vol. V, No. 1, 1947, pp. 63-66.

9. Dally, J. W., and Riley, W. F. Experimental Stress Analysis. New York, McGraw-Hill Book Company, 1965.

10. Frocht, M. M., Landsberg, D., and Wang, B. C. "The Effect of Gage Current on Strain Measurement," Proceedings of the Society for Experimental Stress Analysis, Vol. XVI, No. 2, May, 1958, pp. 69-72.

11. deVeubeke, B. F. Matrix Methods of Structural Analysis. (AGARDograph 72), New York, The Macmillan Company, 1964.

12. Bampton, M. C. C. Matrix Structural Analysis. Boeing Company Document No. D6-2587 TN, December, 1964.

APPENDIX I

DETERMINATION OF MECHANICAL PROPERTIES OF PLEXIGLAS

The model selected for determining the mechanical properties was a single-cell cantilever box beam with glued joints. The beam was twenty inches long, two inches wide, and two inches in depth, with all sides constructed of 0.125 inch thick plexiglas. Transverse ribs were located every two inches along the beam for stability purposes. The plexiglas and adhesive used in this model are the same as those used in the construction of the basic model of the text. Single element type A-7 strain gages were cemented on the upper and lower cover plates one inch from the built-in end, and one FABR-12-12 strain gage rosette was located three inches from the built-in end.

Loads were applied at the free end of the beam, and strain measurements were obtained by the use of a Baldwin SR-4 Strain Indicator, Type M. Several tests were made at temperatures varying between 68^{o} and 74^{o} Fahrenheit with negligible difference in all readings.

Figure I-1 depicts the results obtained from the type A-7 strain gages. Strain readings were taken three minutes after load application to allow for the creep rate to be minimized. The creep response for constant stress (Figure I-2) was also obtained from the type A-7 strain gages. As a result of this test it was decided that the stress level should be kept under 500 psi due to the increased creep rate

FIG. I-1
TENSION vs COMPRESSION
TEST TO DETERMINE
MODULUS OF ELASTICITY

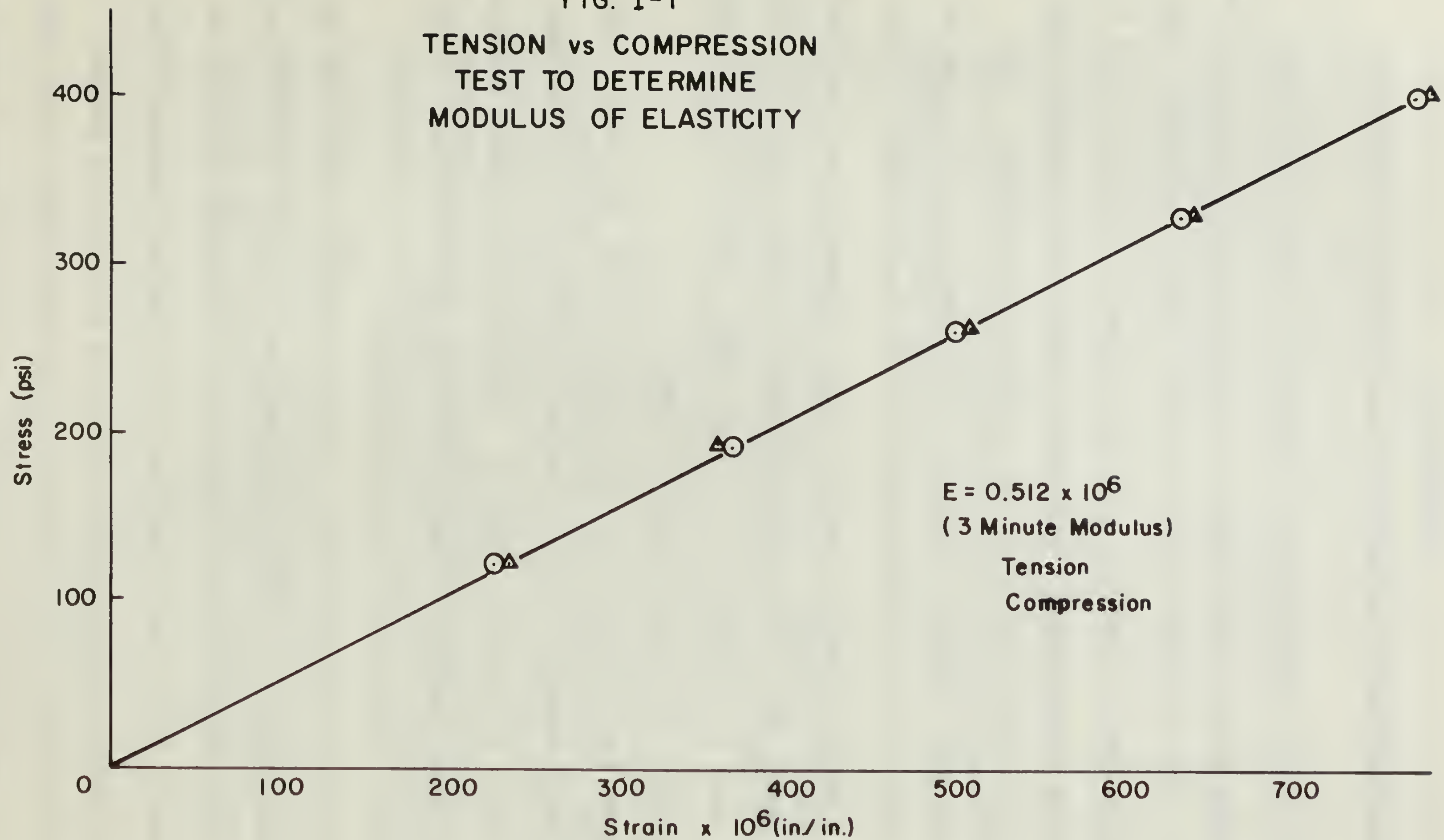

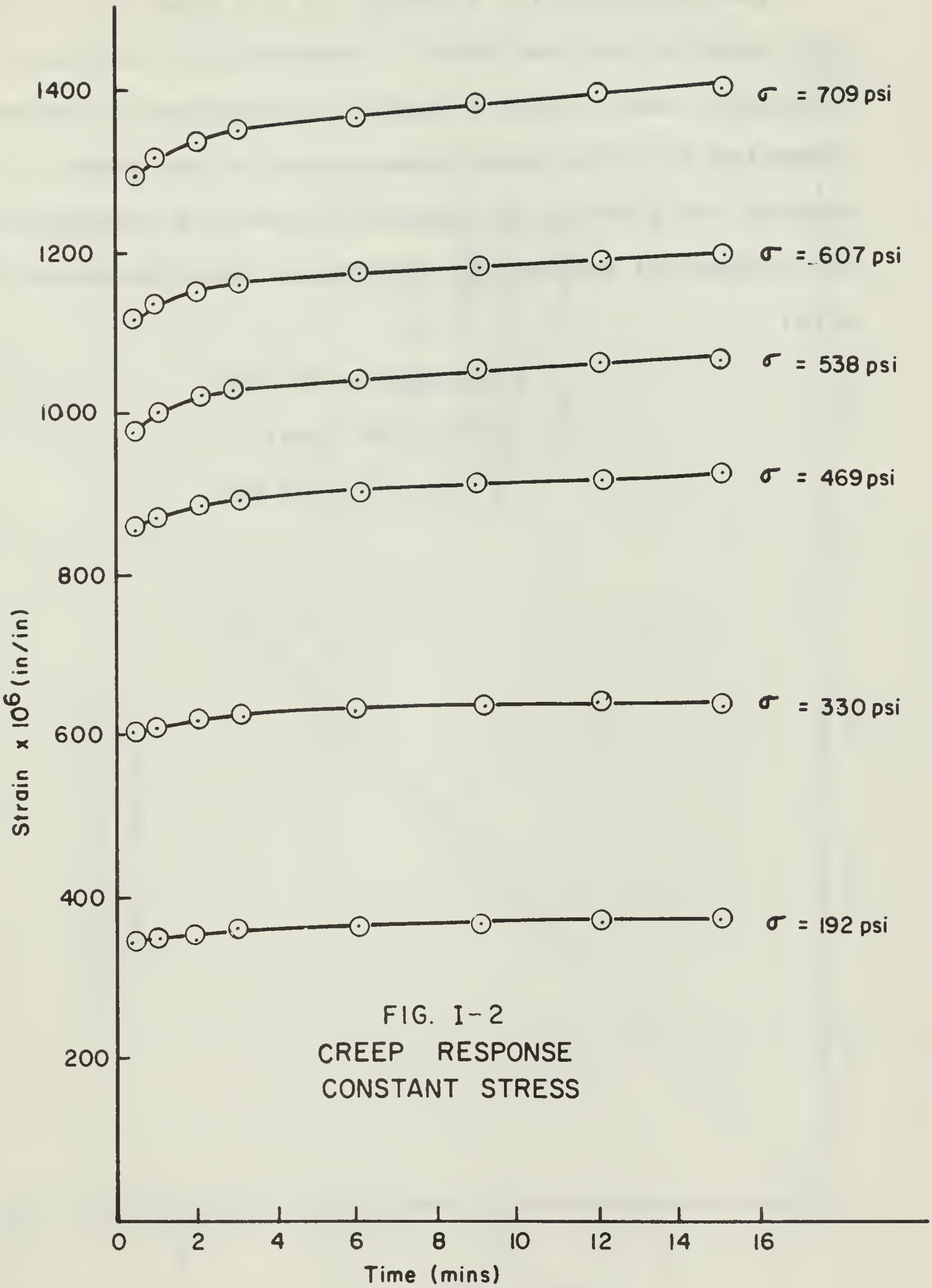

FIG. I-2
CREEP RESPONSE
CONSTANT STRESS

at higher stress levels and that strain readings should be taken at ten minute intervals rather than three minutes.

The perpendicular elements of the FABR-12-12 strain gage rosette were employed to determine the modulus of elasticity and Poisson's Ratio. All measured strains were corrected for transverse sensitivity of the gages. The results are plotted in Figures I-3 and I-4 respectively. The mechanical properties determined from the above tests were:

$$E = 4.85 \times 10^5 \text{ psi}$$

$$\mu = 0.384 \text{ in/in}$$

$$G = 1.75 \times 10^5 \text{ psi}$$

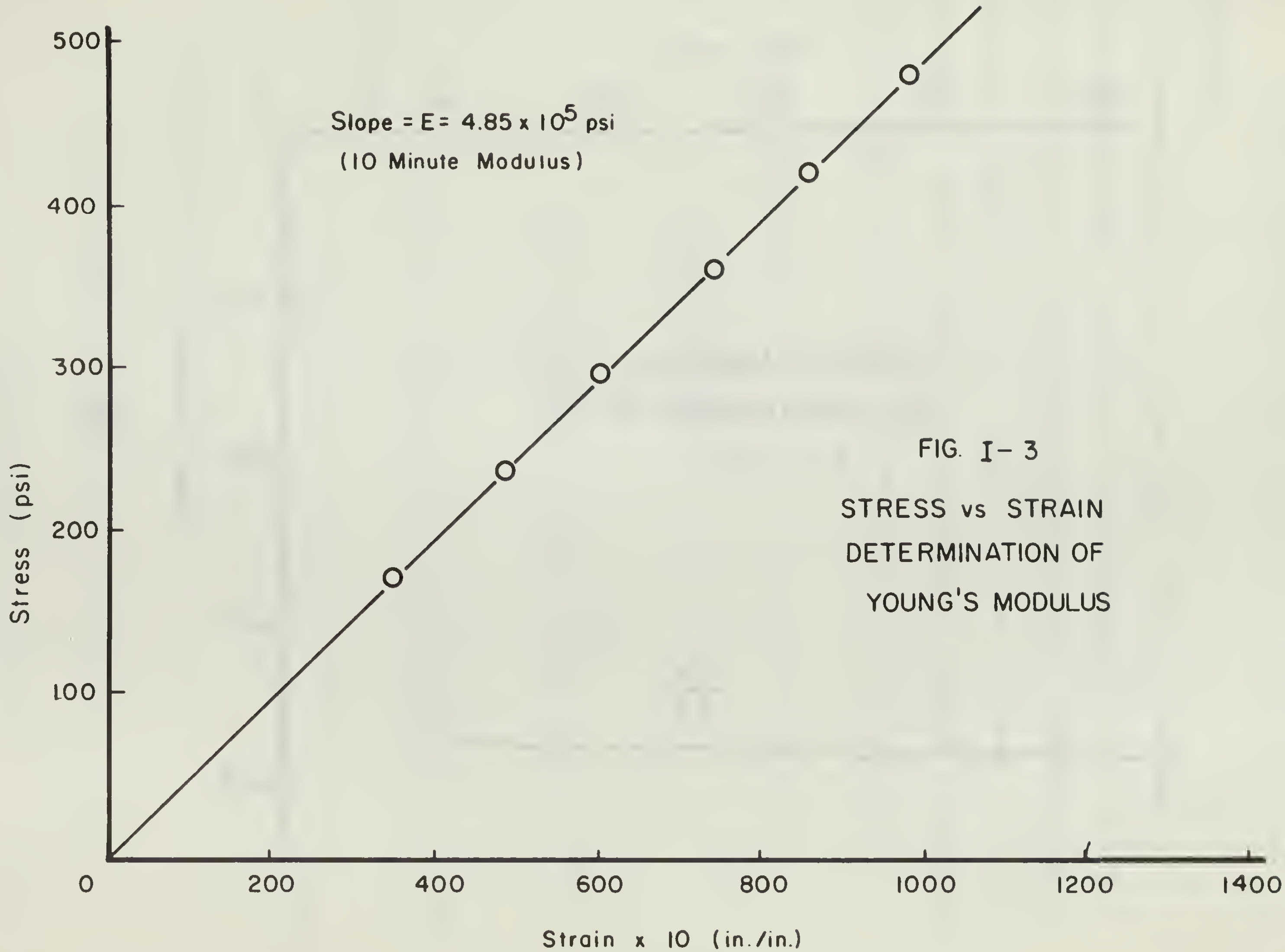

FIG. I-3

STRESS vs STRAIN
DETERMINATION OF
YOUNG'S MODULUS

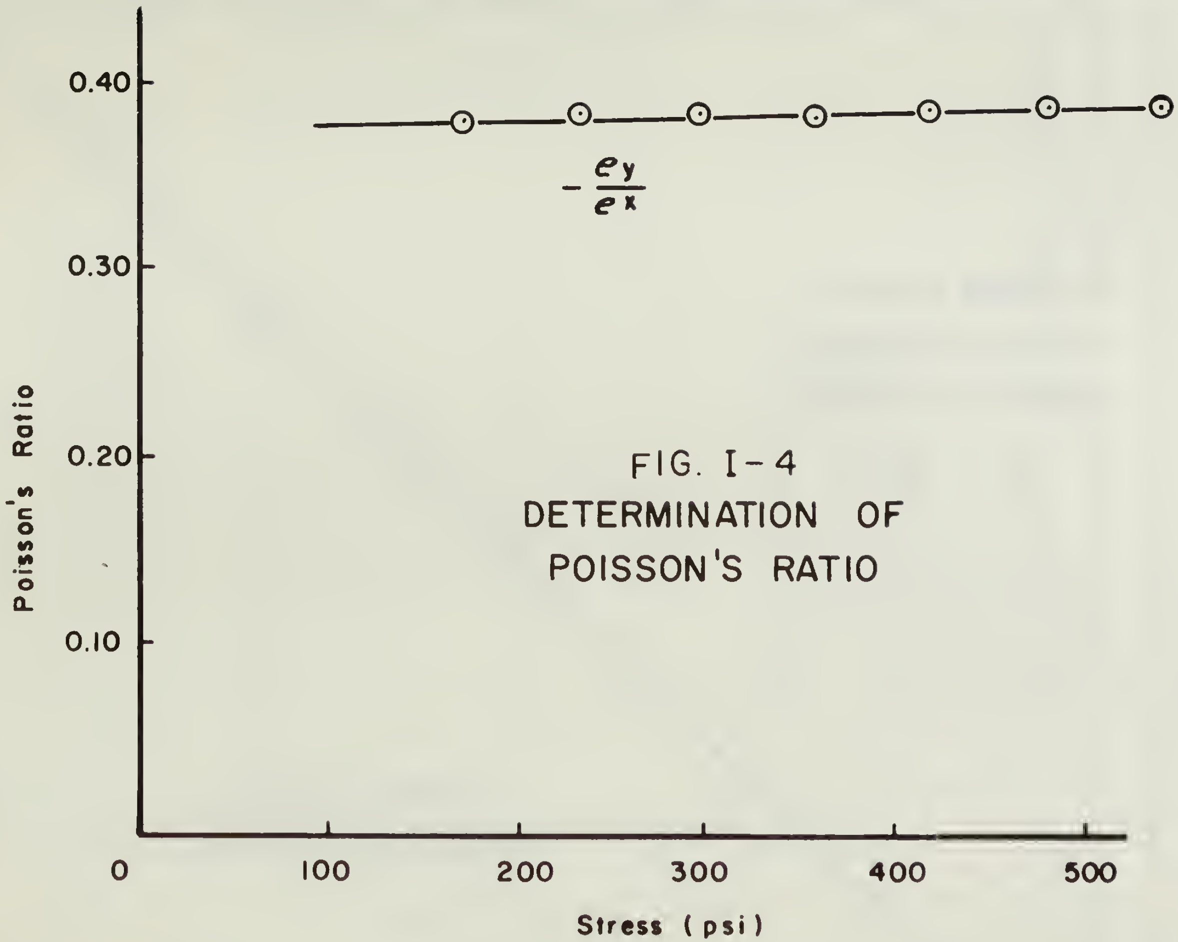

FIG. I-4
DETERMINATION OF
POISSON'S RATIO

APPENDIX II

DESIGN EQUATIONS FOR STRUCTURAL SIMILARITY

<u>Discussion</u>

A structural model is one that, although not necessarily geometrically similar to its prototype, will faithfully reproduce, to some predetermined scale, the required structural characteristics. These may be stresses, strains, deflections, and/or combinations thereof. Design equations relating deflections and stresses are summarized below:

Axial Deflections

$$N_1 \frac{P_m L_m}{A_m E_m} = \frac{P_p L_p}{A_p E_p}$$

$$A_m = N_1 \frac{P_m L_m E_p}{P_p L_p E_m} A_p = \frac{1}{N_f} \frac{E_p}{E_m} A_p \qquad \text{(II-1)}$$

If the model is a complete geometric duplication of the prototype,

$$N_f = \frac{E_p}{E_m} \qquad \text{(II-1a)}$$

Bending Deflections

$$N_1 \frac{P_m L_m^3}{E_m I_m} = \frac{P_p L_p^3}{E_p I_p}$$

$$I_m = N_1 \frac{P_m L_m^3}{P_p L_p^3} \frac{E_p}{E_m} I_p = \frac{1}{N_f N_1^2} \frac{E_p}{E_m} I_p \qquad \text{(II-2)}$$

For complete geometric duplication,

$$N_f = \frac{E_p}{E_m} \tag{II-2a}$$

Torsional Deflections

$$\frac{T_m L_m}{G_m J_m} = \frac{T_p L_p}{G_p J_p}$$

$$J_m = \frac{T_m L_m G_p}{T_p L_p G_m} J_p = \frac{1}{N_1} \frac{T_m G_p}{T_p G_m} J_p \tag{II-3}$$

For complete geometric duplication,

$$\frac{T_p}{T_m} = N_f = \frac{G_p}{G_m} = \frac{E_p \ (1 + \mu m)}{E_m \ (1 + \mu p)} \tag{II-3a}$$

Bending and Twisting Moments

$$\frac{M_m}{M_p} = \frac{P_m L_m}{P_p L_p} = \frac{1}{N_f N_1} \tag{II-4}$$

For complete geometric duplication,

$$\frac{M_m}{M_p} = \frac{1}{N_f} \tag{II-4a}$$

Axial Stresses

$$\frac{\sigma_m}{\sigma_p} = \frac{\frac{P_m}{A_m}}{\frac{P_p}{A_p}} = \frac{P_m A_p}{P_p A_m} = \frac{{N_1}^2}{N_f} \tag{II-5}$$

For complete geometric duplication,

$$\frac{\sigma_m}{\sigma_p} = \frac{1}{N_f} \tag{II-5a}$$

Bending Stresses

$$\frac{\sigma_m}{\sigma_p} = \frac{\dfrac{M_m c_m}{I_m}}{\dfrac{M_p c_p}{I_p}} = \frac{M_m c_m I_p}{M_p c_p I_m} \tag{II-6}$$

For complete geometric duplication,

$$\frac{\sigma_m}{\sigma_p} = \frac{M_m}{M_p} = \frac{1}{N_f} \tag{II-6a}$$

Torsional Shear Flow

$$\frac{q_m}{q_p} = \frac{\dfrac{T_m}{2A_m}}{\dfrac{T_p}{2A_p}} = \frac{T_m A_p}{T_p A_m} = \frac{1}{N_f N_l} \; \frac{A_p}{A_m} \tag{II-7}$$

For complete geometric duplication,

$$\frac{q_m}{q_p} = \frac{1}{N_f} \tag{II-7a}$$

In a similar fashion it can be shown that the relationship between any physical quantities can be determined in terms of the basic dimensional parameters.

APPENDIX III

TORSIONAL SHEAR FLOW CALCULATIONS

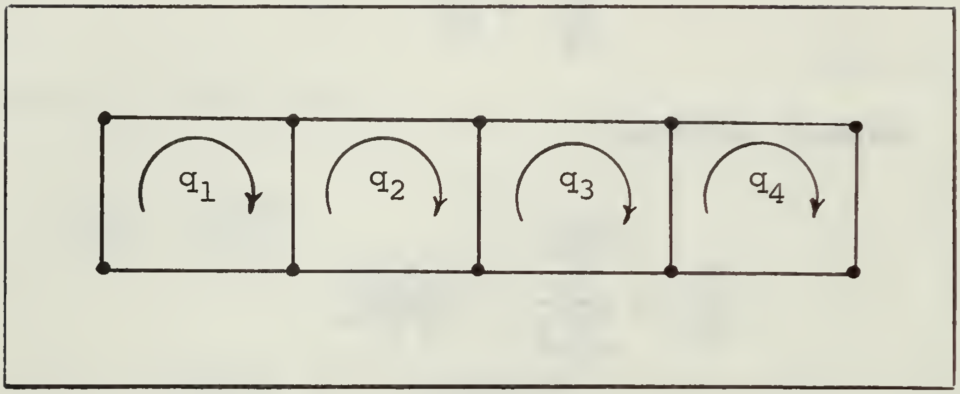

FIG. III-1 SHEAR FLOW AT A TYPICAL CROSS SECTION.

Figure III-1 above is a typical cross section of the model under consideration. The following assumptions have been made:

1. The section is allowed to warp under a torsional deflection (no normal forces).
2. The section is far enough away from the rib root so that sweep angle does not effect the results.
3. The section is infinitely stiff in the chordwise direction (no bending in the chordwise direction).

From assumption 3 above, the torsional deflections for each of the cells are equal. Torsional deflection for a cell is given by

$$\theta = \oint \frac{q \; ds}{2AGt} \qquad \text{(III-1)}$$

Equating the deflections for each cell gives,

$$\oint_1 \frac{q\ ds}{2AGt} = \oint_2 \frac{q\ ds}{2AGt} = \oint_3 \frac{q\ ds}{2AGt} = \oint_4 \frac{q\ ds}{2AGt} \qquad \text{(III-2)}$$

Since $A_1 = A_2 = A_3 = A_4$ and G is constant,

$$\oint_1 \frac{q\ ds}{t} = \oint_2 \frac{q\ ds}{t} = \oint_3 \frac{q\ ds}{t} = \oint_4 \frac{q\ ds}{t}\ . \qquad \text{(III-3)}$$

Let $B_{ii} = \oint \frac{ds_i}{t}$ and $B_{ij} = \int \frac{ds_{ij}}{t}$

where s_i is the total distance around cell i, and s_{ij} is the height of the spar rib between cells i and j.

From the given dimensions of the section,

$$B_{11} = B_{22} = B_{33} = B_{44} = 131.0$$

$$B_{12} = B_{21} = B_{23} = B_{32} = B_{34} = B_{43} = 40.3$$

Substituting the above into equation (III-3) gives a set of simultaneous linear equations in terms of shear flows:

$$B_{11}q_1 - B_{12}q_2 = B_{22}q_2 - B_{21}q_1 - B_{23}q_3$$

$$B_{22}q_2 - B_{21}q_1 - B_{23}q_3 = B_{33}q_3 - B_{32}q_2 - B_{34}q_4$$

$$B_{33}q_3 - B_{32}q_2 - B_{34}q_4 = B_{44}q_4 - B_{43}q_3$$

$$B_{11}q_1 - B_{12}q_2 = B_{44}q_4 - B_{43}q_3$$

Solving the above equations gives,

$$q_1 = q_4$$

$$q_2 = q_3 = \frac{B_{11} + B_{12}}{B_{22}} = 1.31\ q_1$$

The internal torsional moment is given by,

$$T = \sum 2A_i q_i \qquad \text{(III-4)}$$

where i is the cell number. Therefore,

$$T = 2A(q_1 + q_2 + q_3 + q_4)$$

$$= 2A(q_1 + 1.31\ q_1 + 1.31\ q_1 + q_1)$$

$$T = (2)(2.5)(2.95)(4.62)\ q_1 = 68.0\ q_1$$

Equating the above results to the applied external torsional moment gives,

$$(11.8)\ \frac{P}{2} = 68.0\ q_1$$

$$q_1 = 0.0868\ P$$

$$q_2 = 0.1140\ P$$

$$q_{12} = q_{23} = q_2 - q_1 = 0.0272\ P$$

$$q_{23} = q_2 - q_3 = 0$$

Dividing the shear flows by the corresponding panel thicknesses gives the following shear stress distribution:

On the outer cover plate panels,

$$\tau_{xy} = 0.735 \text{ P psi.}$$

On the inner cover plate panels,

$$\tau_{xy} = 0.966 \text{ P psi.}$$

On the outer spar web panels,

$$\tau_{xy} = 1.400 \text{ P psi.}$$

On the next inboard spar web panels,

$$\tau_{xy} = 0.440 \text{ P psi.}$$

The shear stress on the center spar web panel is zero.

The above results are completely theoretical based on the given assumptions. To check the experimental results, substitute the measured shear flows into equation (III-4) above and compare the results with the applied torsional moment.

APPENDIX IV

DETERMINATION OF PRINCIPAL STRESSES AND PRINCIPAL AXES ORIENTATION

The three-element rectangular rosette employs gages placed at the 0°, 45°, and 90° positions, as indicated in Figure IV-1.

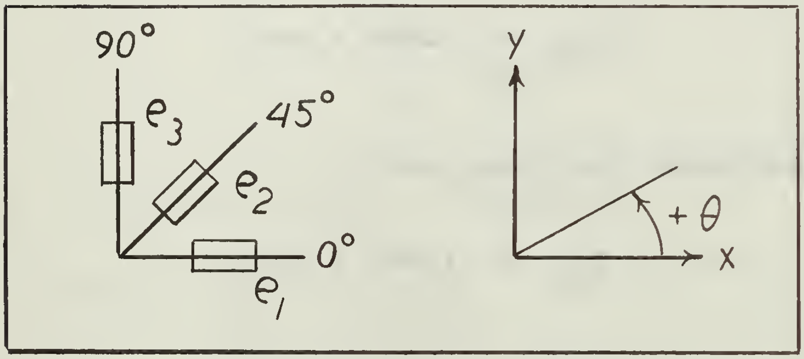

FIG. IV-1 ROSETTE ORIENTATION

For this particular rosette the following relations hold if the 0° and 90° elements coincide with the x and y coordinate axes of the stress field:

$$e_1 = e_{yy}$$

$$e_2 = 1/2\,(e_{xx} + e_{yy} + \gamma_{xy})$$

$$e_3 = e_{xx}$$

$$\gamma_{xy} = 2e_2 - e_1 - e_3$$

This establishes the cartesian components of strain which are used in the following Mohr's circle relationships:

$$e_a = 1/2\ (e_{xx} + e_{yy}) + 1/2 \sqrt{(e_{xx} - e_{yy})^2 + \gamma_{xy}^{\ 2}}$$

$$e_b = 1/2\ (e_{xx} + e_{yy}) - 1/2 \sqrt{(e_{xx} - e_{yy})^2 + \gamma_{xy}^{\ 2}}$$

$$\tan 2\theta = \frac{\gamma_{xy}}{e_{xx} - e_{yy}}$$

where e_a and e_b are the principal strains and θ is the angle between the principal axis and the x axis. The above equation for determining the angle θ has two solutions. The principal axes may be identified by applying the following rules:

$0^\circ < \theta < 90^\circ$	when $e_2 > 1/2(e_1 + e_3)$
$-90^\circ < \theta < 0^\circ$	when $e_2 < 1/2(e_1 + e_3)$
$\theta = 0^\circ$	when $e_1 > e_3$ and $e_1 = e_a$
$\theta = \pm 90^\circ$	when $e_1 < e_3$ and $e_1 = e_b$

These are the relationships used to reduce the data for this analysis with the exception of re-orientation of the e_1 and e_2 axes. Principal stresses may then be obtained from the following equations.

$$\sigma_{max} = \frac{E}{2}\left[\frac{e_1 + e_3}{(1 - \mu)} + \frac{1}{(1 + \mu)}\sqrt{(e_1 - e_3)^2 + \gamma_{xy}^{\ 2}}\right]$$

$$\sigma_{min} = \frac{E}{2}\left[\frac{e_1 + e_3}{(1 - \mu)} - \frac{1}{(1 + \mu)}\sqrt{(e_1 - e_3)^2 + \gamma_{xy}^{\ 2}}\right]$$

INITIAL DISTRIBUTION LIST

		No. Copies
1.	Defense Documentation Center Cameron Station Alexandria, Virginia 22314	20
2.	Library Naval Postgraduate School Monterey, California 93940	2
3.	Commander, Naval Air Systems Command Department of the Navy Washington, D. C. 20360	1
4.	Chairman, Department of Aeronautics Naval Postgraduate School Monterey, California 93940	1
5.	Prof. C. H. Kahr Department of Aeronautics Naval Postgraduate School Monterey, California 93940	3
6.	Prof. U. Haupt Department of Aeronautics Naval Postgraduate School Monterey, California 93940	1
7.	LT J. A. Sheler, USN P. O. Box 17321 San Diego, California 92117	2
8.	Mr. G. L. Desmond Aerodynamics and Structures Technical Administrator Naval Air Systems Command Department of the Navy Washington, D. C. 20360	1
9.	Dr. E. S. Lamar Chief Scientist Naval Air Systems Command Department of the Navy Washington, D. C. 20360	1
10.	Prof. A. E. Fuhs Department of Aeronautics Naval Postgraduate School Monterey, California 93940	1

UNCLASSIFIED

Security Classification

DOCUMENT CONTROL DATA - R&D

(Security classification of title, body of abstract and indexing annotation must be entered when the overall report is classified)

1. ORIGINATING ACTIVITY (Corporate author)	2a. REPORT SECURITY CLASSIFICATION
Naval Postgraduate School Monterey, California	Unclassified
	2b. GROUP

3. REPORT TITLE

Experimental Analysis of a Plastic Model Multicell Cantilever Box Beam With 30° Sweep

4. DESCRIPTIVE NOTES (*Type of report and inclusive dates*)

Masters Thesis

5. AUTHOR(S) (*Last name, first name, initial*)

Sheler, James A., LT, USN

6. REPORT DATE	7a. TOTAL NO. OF PAGES	7b. NO. OF REFS
December 1967	62	12

8a. CONTRACT OR GRANT NO.	9a. ORIGINATOR'S REPORT NUMBER(S)
b. PROJECT NO.	
c.	9b. OTHER REPORT NO(S) (*Any other numbers that may be assigned this report*)
d.	

10. AVAILABILITY/LIMITATION NOTICES

[redacted] ~~subject to special export controls and each~~ [redacted] ~~to foreign governments or foreign nationals may be made~~ [redacted] ~~approval of the U.S. Naval Postgraduate School.~~

11. SUPPLEMENTARY NOTES	12. SPONSORING MILITARY ACTIVITY
	Naval Postgraduate School Monterey, California

13. ABSTRACT

An experimental analysis of a plastic model four-cell swept back wing is presented. The model is cantilevered with a massive root rib oriented 60° with the spars. Three other ribs are located perpendicular to the spars. The results were compared with results previously obtained from tests performed on an aluminum alloy model of the same structure. Spanwise stresses and deflections compared very well. Considerable error was observed in chordwise stresses and shear stresses due to lack of joint duplication at the root rib and a difference in Poisson's Ratio between the two materials.

DD FORM 1 JAN 64 1473

UNCLASSIFIED

Security Classification

14 KEY WORDS	LINK A		LINK B		LINK C	
	ROLE	WT	ROLE	WT	ROLE	WT
Swept back wing						
Plastic model						
Stress						

[redacted]